Universal signatures of Fermi arcs in quasiparticle interference on the surface of Weyl semimetals

Stefanos Kourtis, Jian Li, Zhijun Wang, Ali Yazdani, and B. Andrei Bernevig

Phys. Rev. B **93**, 041109 — Published 26 January 2016

DOI: 10.1103/PhysRevB.93.041109

Universal signatures of Fermi arcs in quasiparticle interference on the surface of Weyl semimetals

Stefanos Kourtis, Jian Li, Zhijun Wang, Ali Yazdani, and B. Andrei Bernevig
Department of Physics, Princeton University, Princeton, NJ 08544, USA
(Dated: January 5, 2016)

Weyl semimetals constitute a newly discovered class of three-dimensional topological materials with linear touchings of valence and conduction bands in the bulk. The most striking property of topological origin in these materials, so far unequivocally observed only in photoemission experiments, is the presence of open constant-energy contours at the boundary — the so-called Fermi arcs. In this work, we establish the universal characteristics of Fermi-arc contributions to surface quasiparticle interference. Using a general phenomenological model, we determine the defining interference patterns stemming from the existence of Fermi arcs in a surface band structure. We then trace these patterns in both simple tight-binding models and realistic ab initio calculations. Our results show that definitive signatures of Fermi arcs can be observed in existing and proposed Weyl semimetals using scanning tunneling spectroscopy.

I. INTRODUCTION

The prototypical examples of noninteracting topological states of matter are categorized by quantized invariants, corresponding to (sets of) energy bands that are separated by gaps from the rest of the band structure. A conceptual step forward in the topological characterization of materials was the definition of topological invariants for systems in which energy gaps vanish and bands touch[1]. For example, in the presence of inversion and time-reversal, two-dimensional spinless graphene exhibits a quantized topological invariant. In the vicinity of isolated points in the Brillouin zone, where Dirac nodes occur, the topological invariant is obtained by integrating the Berry potential over a closed line encircling these points.

Similarly, in three dimensions, nodes may appear in pairs of opposite chirality, i.e., as sources and sinks of Berry flux[1–5]. The two nodes in each pair can be pushed apart in reciprocal space by breaking the product of time reversal and inversion symmetries. The low-energy theory describing electrons at such a nodal point is encapsulated in the Weyl equation. When the chemical potential crosses or is close to these nodal points in a material, the latter is called a Weyl semimetal (WSM)[6–9]. Unlike Dirac nodes in graphene, Weyl nodes cannot be gapped or otherwise removed from the band structure by small translation-symmetry preserving perturbations. When a closed Fermi surface (FS) patch encloses only one Weyl node, one can define a FS Chern number, which is equal to the topological charge of the node[10–13].

Recently, experimental evidence for the discovery of Weyl fermions in TaAs and NbAs was provided by angle-resolved photoemission spectrocopy[14–18] and (magneto)transport measurements[19,20]. The theory that guided the discovery[21,22] attracted immediate attention, because the materials are stoichiometric and therefore easy to synthesize. The prediction of a second type of WSMs rendered another two compounds, WTe_2 and $MoTe_2$, promising candidates for realization[23–25].

One of the most interesting hallmarks of a WSM is the presence of open constant-energy contours in its surface band structure called Fermi arcs[6,7]. The existence of the corresponding surface states is a direct consequence of the nonzero topological charge associated with a Weyl node. Since they pertain solely to the surface, these previously elusive FS features are also amenable to observation via scanning tunneling spectroscopy (STS). An analysis of quasiparticle-interference (QPI) patterns in the Fourier-transformed local density of states (FTLDOS) at the boundary of a material can yield important properties of surface quantum states[26–35]. The potential for detecting Fermi arcs with STS was recognized in earlier theoretical work[36,37], but the QPI fingerprints of Fermi arcs remain theoretically and experimentally unresolved.

The purpose of the present manuscript is to determine the unique signatures of Fermi arcs in the QPI patterns obtained by STS measurements at the surface of a WSM. First, we identify the most elementary QPI pattern shapes in the presence of a single Fermi arc and define criteria for their unambiguous experimental observation. Since both discovered and candidate WSMs host two or more pairs of Weyl nodes and will hence have more than one Fermi arcs on a given surface, we examine the fundamental QPI features when more than one arcs coexist on the same surface. In the case of type-2 WSMs, the boundary FS will comprise of both Fermi arcs and electron and hole pockets. We therefore study the fate of the nontrivial characteristics in QPI when surface modes are allowed to scatter into states originating from the bulk. We then pinpoint all aforementioned signatures in QPI patterns obtained from both generic tight-binding models and density functional theory (DFT) calculations for $MoTe_2$ and TaAs.

II. THEORY OF QPI AT THE SURFACE OF WEYL SEMIMETALS

A. Definition of QPI response

The FTLDOS obtained from STS measurements can be generally expressed as[38,39]

$$F(\boldsymbol{q},E) = \frac{i}{2\pi}[\Lambda(\boldsymbol{q},E) - \Lambda(-\boldsymbol{q},E)^*], \tag{1}$$

$$\Lambda(\boldsymbol{q},E) = \int \mathrm{d}\boldsymbol{k}\, \mathrm{Tr}[G(\boldsymbol{k}+\boldsymbol{q},E)T(\boldsymbol{k}+\boldsymbol{q},\boldsymbol{k};E)G(\boldsymbol{k},E)]\,, \tag{2}$$

where $G(\boldsymbol{k},E)$ is the retarded Green's function for a clean sample and $T(\boldsymbol{k},\boldsymbol{k}';E)$ is the T-matrix associated with disorder[40]. On heuristic grounds, the power spectrum $|F(\boldsymbol{q},E)|$ is

commonly approximated by the autocorrelation of the spectral functions[28,41,42]

$$J_\nu(\boldsymbol{q}, E) = \int \mathrm{d}\boldsymbol{k}\, \mathrm{Tr}[A_\nu(\boldsymbol{k}+\boldsymbol{q}, E) A_\nu(\boldsymbol{k}, E)], \quad (3)$$

$$A_\nu(\boldsymbol{k}, E) = (i/2\pi)\mathrm{Tr}_{\bar{\nu}}[G(\boldsymbol{k}, E) - G(\boldsymbol{k}, E)^\dagger], \quad (4)$$

where ν stands for the set of inner degrees of freedom that is preserved in the scattering (e.g. spin in spin-preserving scattering), and $\mathrm{Tr}_{\bar{\nu}}$ stands for the partial trace over all inner degrees of freedom other than ν, such that A_ν is a reduced density matrix in terms of ν. In this work, we will consider two types of autocorrelations: the joint density of states (JDOS) J_0 with ν being an empty set, and the spin-dependent scattering probability (SSP) J_s with ν being solely electron spin. The JDOS is particularly important in studying a WSM that lacks any symmetry — this is the most generic WSM although it is still to be found experimentally; the SSP includes suppressions due to the symmetries of the eigenstates and is hence important for WSMs that respect time-reversal symmetry — the case for all confirmed WSMs.

The JDOS ignores all matrix-element effects inherent in FTLDOS and takes into account all energetically allowed scattering wavevectors on equal footing, whereas SSP includes only the scattering suppression that comes from the spin content of the wavefunction. Approximating FTLDOS with JDOS / SSP amounts to replacing the impurity landscape with a single scattering center, which can be easily treated within band theory. Even though the rationale behind evaluating JDOS / SSP instead of the full FTLDOS is clear, it is not always straightforward to rigorously connect one to the other[39]. For this reason, we have verified that our key findings based on JDOS / SSP calculations are qualitatively the same in the full FTLDOS of our tight-binding models[43].

B. Phenomenology

Let us now consider the JDOS patterns most broadly associated with Fermi arcs. First, we illustrate the key points phenomenologically, by assuming that the Fermi arcs have a constant curvature and a constant spectral density. The Fermi level is supposed to cross the bulk band structure only at the nodal points, so that only boundary modes are visible in the surface FS. The spectral function of an individual arc at a fixed energy can be parametrized as

$$A(\boldsymbol{k}; \boldsymbol{k}_1, r_1, \gamma_1, \varphi_1) = \int_{\varphi_1}^{\varphi_1+\gamma_1} \mathrm{d}\varphi\, \delta(\boldsymbol{k} - \boldsymbol{k}_1 - r_1(\cos\varphi, \sin\varphi)), \quad (5)$$

where $\boldsymbol{k}_1$ is the offset of the circle center from the origin, r_1 the circle radius and γ_1 the angle subtended by the arc. The endpoints of the arc are located at $r_1(\cos\varphi_1, \sin\varphi_1)$ and $r_1(\cos(\varphi_1+\gamma_1), \sin(\varphi_1+\gamma_1))$. The JDOS generated solely by this single arc is independent of $\boldsymbol{k}_1$, while r_1 and φ_1 change only its size and orientation, respectively. The only parameter that affects the shape of the arc is γ_1. This is shown in Fig. 1(a-d) for three idealized, perfectly circular, cases. Figs. 1(e,f) illustrate the autocorrelation of a FS that includes a second arc. Apart from the feature that arises from the autocorrelations of the two arcs, which is exactly like that of Fig. 1(b), there are now cross-correlation patterns at finite momenta, corresponding to scattering between arcs.

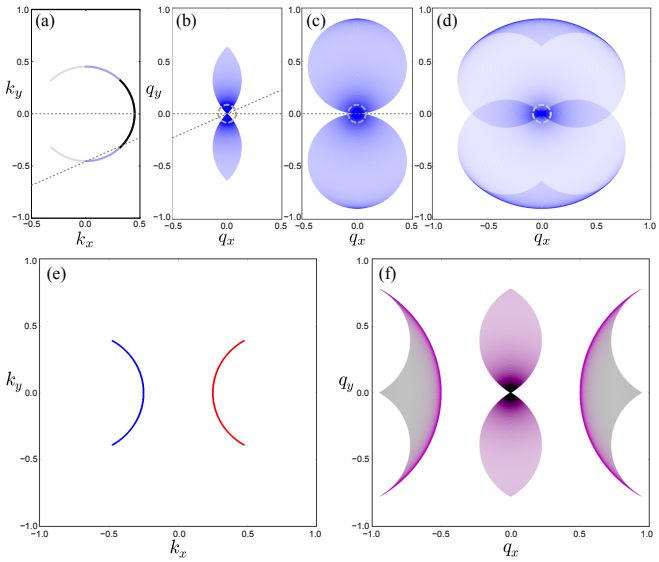

FIG. 1. (a-d) Single Fermi arc (a) parametrized by Eq. (5) with $r_1 = 0.45$, $\boldsymbol{k}_1 = 0$, $\gamma_1 = -2\varphi_1$ and the shape of its corresponding JDOS from Eq. (3) for (b) $\varphi_1 = -\pi/4$, (c) $\varphi_1 = -\pi/2$ and (d) $\varphi_1 = -3\pi/4$. (e) Two Fermi arcs with $\gamma_1 = \gamma_2 = 2\pi/3$ and (f) the shape of the corresponding JDOS. In (a-d), dashed lines encircle the pinch points; dotted lines are described in the text.

The most distinctive feature is the presence of a pinch point at $\boldsymbol{q} = 0$ for arcs with $\gamma_1 \leq \pi$. This is a unique characteristic of an open contour in the surface BZ and can be interpreted as follows: a pinch point exists as long as scattering within a FS contour vanishes at all wavevectors along a specific direction. When such a pinch point exists in the QPI pattern, then the contour that generates it must be open. Consider a translation of the spectral function of an arc defined as $\mathcal{T}_{\epsilon\boldsymbol{v}} A(\boldsymbol{k}) = A(\boldsymbol{k} + \epsilon\boldsymbol{v})$, with $\boldsymbol{v}$ a unitary vector defining a direction in $\boldsymbol{k}$-space and $\epsilon \in \mathbb{R}$. A pinch point exists if there is a $\boldsymbol{v}$ such that $A(\boldsymbol{k})\mathcal{T}_{\epsilon\boldsymbol{v}} A(\boldsymbol{k}) = 0$ for any $\epsilon \neq 0$, so that, from Eq. (3), $J_0(\boldsymbol{q} = \epsilon\boldsymbol{v}) = 0$. The directions $\boldsymbol{v}$ for which this property holds are revealed by the orientation of the resulting pattern in J_0. This is illustrated by the examples in Figs. 1(a-c): a translation of the arc with $\gamma_1 = \pi/2$ [shown in black in Fig. 1(a)] along either of the two dotted lines in Fig. 1(a) leads to $A(\boldsymbol{k})\mathcal{T}_{\epsilon\boldsymbol{v}} A(\boldsymbol{k}) = 0$. Translated to the origin, the same lines cross the autocorrelation pattern Fig. 1(b) only at the pinch point. For $\gamma_1 = \pi$, the above holds only for $\boldsymbol{v} = \hat{\boldsymbol{x}}$, the unitary vector in the x direction. For $\gamma_1 > \pi$, this property does not hold: $A(\boldsymbol{k})\mathcal{T}_{\epsilon\boldsymbol{v}} A(\boldsymbol{k}) \neq 0$ for small ϵ along any $\boldsymbol{v}$. Nonetheless, a pinch point can still be found in the autocorrelation of an arc with $\gamma_1 > \pi$: one can simply split it into two arcs, the first one with $\gamma_1' = \pi$ and a second one with the residual angle $\gamma_1 - \gamma_1'$. The autocorrelation of the first part

generates the pattern in Fig. 1(c), while the autocorrelation of the residue is similar to Fig. 1(b) with a pinch point at $\boldsymbol{q} = 0$. The pinch point in this case, however, is on top of the pattern stemming from γ_1' and the cross-correlation between the two parts [see Fig. 1(d)]. Even though for the purpose of illustration we employed circular arcs, the translation condition for the presence of a pinch point in J_ν is general and can be used regardless of the arc shape. We shall recover this feature in both tight-binding and DFT calculations below. We remark that, even though the $\boldsymbol{q} \simeq 0$ region may be difficult to resolve in QPI experiments, identification of the 8-figure pattern at larger $\boldsymbol{q}$, like the ones in Figs. 1(b,c,f), indicates a pinch point at $\boldsymbol{q} = 0$.

C. Tight-binding formulation

The simplest tight-binding formalism for WSMs is given by the Hamiltonian

$$\mathcal{H} = \sum_{\boldsymbol{k}} \psi^\dagger_{\boldsymbol{k}} H(\boldsymbol{k}) \psi_{\boldsymbol{k}} \,, \tag{6}$$

where $\psi_{\boldsymbol{k}} = (c_{\boldsymbol{k},A,\uparrow}\ c_{\boldsymbol{k},A,\downarrow}\ c_{\boldsymbol{k},B,\uparrow}\ c_{\boldsymbol{k},B,\downarrow})^{\mathsf{T}}$ is a fermionic spinor containing electronic annihilation operators $c_{\boldsymbol{k},s,\sigma}$, with $s = A, B$ orbital/sublattice and $\sigma = \uparrow, \downarrow$ spin indices respectively, and $\psi^\dagger_{\boldsymbol{k}}$ its hermitian conjugate. Let us first ignore the spin degree of freedom. In this case, we can write a minimal (two-component) tight-binding model describing a WSM with only two Weyl nodes as

$$H_{2\times2}(\boldsymbol{k}) = \boldsymbol{g}(\boldsymbol{k}) \cdot \boldsymbol{\tau} + g_0(\boldsymbol{k})\tau_0 \,, \tag{7a}$$

where $\boldsymbol{\tau}$ is the vector of Pauli matrices and τ_0 the 2×2 unity matrix in orbital/sublattice space, $\boldsymbol{g} = (g_1, g_2, g_3)$ and

$$g_0(\boldsymbol{k}) = 2d(2 - \cos k_x - \cos k_y) \,, \tag{7b}$$
$$g_1(\boldsymbol{k}) = a \sin k_x \,, \tag{7c}$$
$$g_2(\boldsymbol{k}) = a \sin k_y \,, \tag{7d}$$
$$g_3(\boldsymbol{k}) = m + t\cos k_z + 2b(2 - \cos k_x - \cos k_y) \,, \tag{7e}$$

with a, b, d, m, t real parameters ($a, t \neq 0$). With $b = d = 0$ and $|m| < |t|$, the energy spectrum has 8 Weyl nodes at points given by $k_{x/y} = 0, \pi$ and $k_z = \pm \arccos \frac{m}{t}$. A finite b can gap the nodes with $k_{x/y} = \pi$, so that for $|m + 4b| > |t|$ there are exactly two Weyl nodes at $(0, 0, \pm \arccos \frac{m}{t})$. If one introduces a boundary, a Fermi arc connects the projections of the nodal points on the boundary FS and d controls the curvature of the arc.

To investigate inter-arc scattering that is subject to time-reversal symmetry, we use the four-spinor $\psi_{\boldsymbol{k}}$ and construct the following Hamiltonian

$$\begin{aligned} H_{4\times4}(\boldsymbol{k}) = {} & g_1(\boldsymbol{k})\tau_1\sigma_3 + g_2(\boldsymbol{k})\tau_2\sigma_0 + g_3(\boldsymbol{k})\tau_3\sigma_0 \\ & + g_0(\boldsymbol{k})\tau_0\sigma_0 + \beta\tau_2\sigma_2 + \alpha \sin k_y \tau_1\sigma_2 \,, \end{aligned} \tag{8}$$

where α, β are real parameters, σ_0 and $\sigma_1, \sigma_2, \sigma_3$ are the 2×2 identity and Pauli matrices spanning the spin degree of freedom and a tensor product between τ and σ matrices is assumed. This model produces four Weyl nodes and two Fermi arcs per surface in a finite parameter regime.

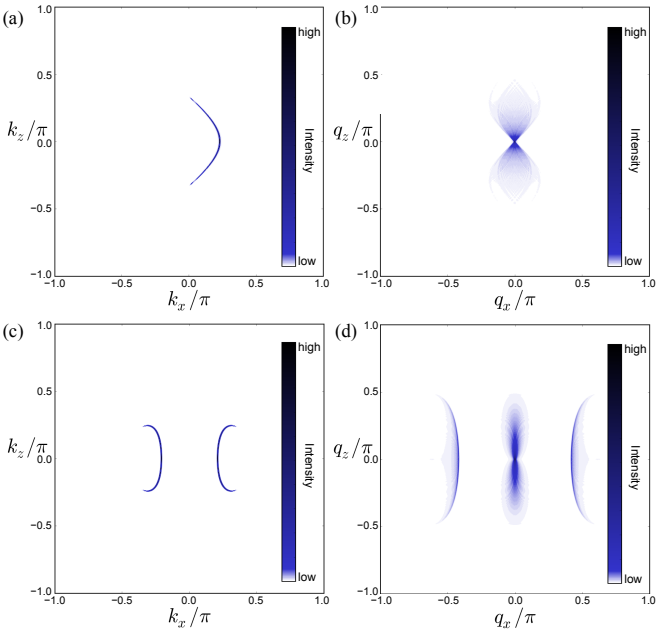

FIG. 2. (a,c) Fermi surfaces ($E = 0$) projected to the (010) surface; (b) JDOS for (a); (d) SSP for (c). The model for (a) and (b) is Eqs. (7) with $a = b = t = 1$, $m = 0.5$, $d = 0.8$; the model for (c) and (d) is Eq. (8) with $a = b = 1$, $t = 1.5$, $d = m = 0$, $\beta = 0.9$ and $\alpha = 0.3$. The JDOS of (c), not shown here, is similar to (d) but shows significantly stronger inter-arc scattering intensity.

Our results for J_0 and J_s, for one and two Fermi arcs yielded by Eqs. (7) and Eqs. (8) respectively, are shown in Fig. 2[43]. The characteristic "8-figure" encountered in the previous section is evident here as well, but its intensity is modulated in accordance with the Fermi-arc DOS, which causes a fading of the pattern at larger $\boldsymbol{q}$. In the case of $H_{4\times4}(\boldsymbol{k})$, the suppression due to the spin texture of the two Fermi arcs has been taken into account. As can be seen in the resulting QPI pattern Fig. 2(d), there is no qualitative change to the intra-arc scattering intensity, whereas now inter-arc cross-correlation patterns are present [cf. Fig. 1(f)], even though the spin content of the wavefunction causes their partial suppression.

D. Density functional theory

Finally, we present results for QPI in the experimentally discovered WSMs based on density-functional theory (DFT). First, we focus on $MoTe_2$, which was recently proposed as a candidate for a type-2 WSM[24,25]. The band structure obtained in ab initio calculations features four Weyl nodes at points $(\pm0.1011, \pm0.0503, 0)$ in units of reciprocal lattice vectors. This renders the plane $k_y = 0$ to be topologically Z_2 nontrivial, exhibiting a Quantum Spin Hall effect. The result of this QSH is to give rise to two Fermi arcs per surface. By its definition, a type-2 WSM will have a surface DOS that comprises of both Fermi arcs and bulk states projected to the boundary, which is shown in Fig. 3(a). As depicted in Fig. 3(b), contributions to the JDOS from both types of features are superim-

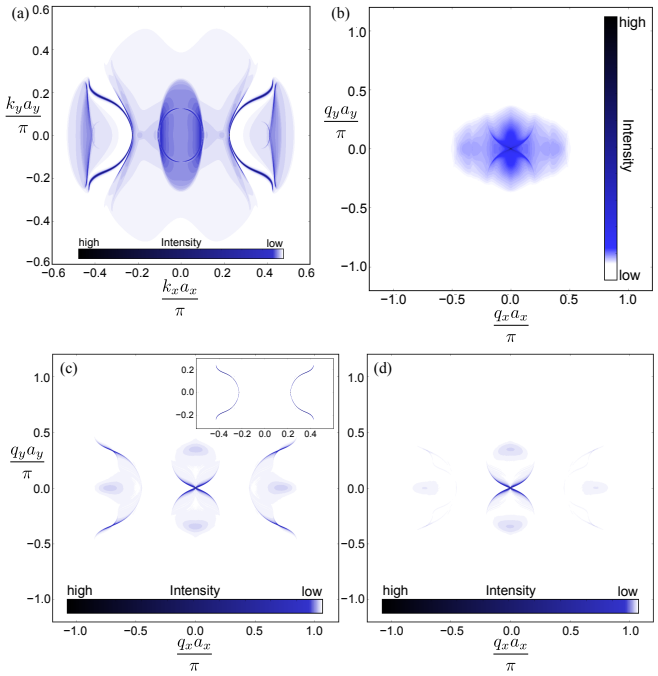

FIG. 3. (a) Surface FS and (b) SSP for the (001) surface of $MoTe_2$ at $E = -0.05$ eV; (c) JDOS for the surface DOS at $\boldsymbol{k}$-points where the intensity is not lower than 10% of the maximum, i.e., keeping only the Fermi arcs shown in the inset of (c); (d) SSP for inset of (c).

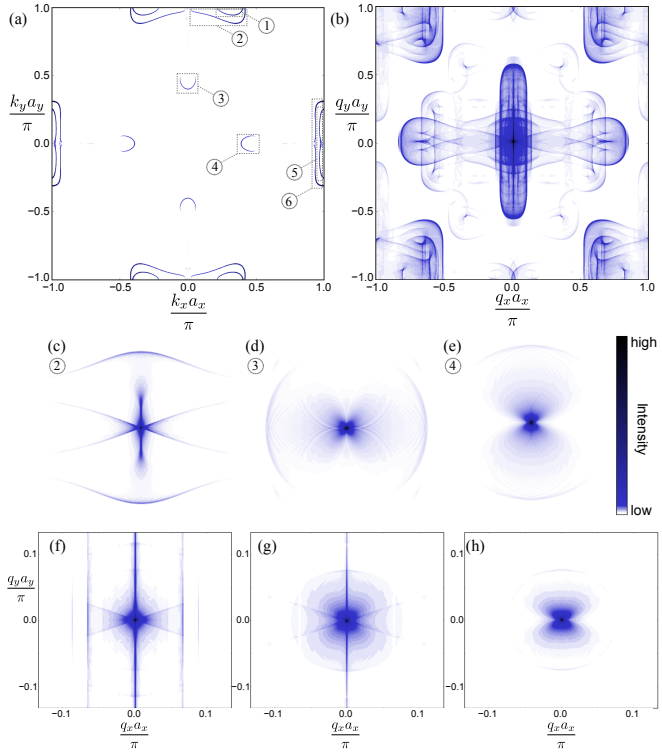

FIG. 4. (a) Surface FS and (b) SSP for the (001) surface of TaAs at $E = 0.12$ eV; (c-e) autocorrelation of DOS features numbered in (a) — cf. Figs. 1(b) and 2(b); (f) SSP close to $\boldsymbol{q} = 0$; (g) SSP close to $\boldsymbol{q} = 0$ minus SSPs centered at $(\pm 2\pi, 0)$ and $(0, \pm 2\pi)$[43]; (h) sum of autocorrelations of features numbered 3 and 4 and their symmetric partners. The intensity of feature 4 is more than two times that of feature 3, so the pattern in (h) is mostly due to the former.

posed. Nevertheless, due to the fact that the states of Fermi arcs are more localized on the surface and have a larger intensity compared to the bulk states that participate in the surface DOS, we recover a clear signature of the Fermi arcs in the JDOS in the form of an "X"-shaped scar. To positively identify this signature, in Fig. 3(c) we show the JDOS obtained if we "mask out" all the bulk signal in the surface DOS. The resulting pattern, which matches the "X"-shaped feature in Fig. 3(b) perfectly, is closely resemblant of Figs. 1(f) and 2(d). Taking spin suppression into account [see Fig. 3(d)] does not alter this result significantly: both intra- and inter-arc features are present in the QPI pattern, although the inter-arc part is weaker. This observation shows that it is possible to distill the contribution of Fermi arcs in the surface QPI spectrum, especially for large Fermi arcs, even if the latter comprises of overlapping patterns stemming from arcs and other FS features.

Next, we investigate the calculated QPI patterns for TaAs. This material has a more complex surface band structure with several Fermi arcs on the (001) surface [21,22,44]. The surface DOS obtained from DFT and the corresponding QPI patterns corresponding to the first BZ are presented in Fig. 4. At $E = 0.12$ eV bulk contributions to the surface DOS are almost completely suppressed. The FS comprises of 12 Fermi arcs (features 2, 3, 4, 6 and their symmetric copies in Fig. 4) and a smaller number of other, non-topological surface features[45]. The bow-tie shaped arcs numbered 2 and 6 extend into the second BZ. With sufficiently high resolution data on a high quality sample all the contributions of the arcs to the QPI should be observable and comparable to our theory. Here, as the γ_1 angle of the weaker spoon-like features 3 and 4 is less than π, we focus on identifying the signatures associated with their intra-arc scattering. We can partially isolate their contributions close to $\boldsymbol{q} = 0$ using only the SSP, as described in the Supplemental Material[43]. With this procedure, we can resolve the 8-figure pattern and pinch point on top of bow-tie contributions, as shown in Figs. 4(g,h). However, it is likely that the small spoon features observed in our calculation may be obscured by long wavelength variations that typically complicate the analysis of STM QPI data at small $\boldsymbol{q}$.

III. CONCLUSION

In conclusion, we have identified signatures of Fermi arcs in quasiparticle interference at the surface of WSMs. We have observed a characteristic 8-figure shape with a pinch point in its middle in both general tight-binding models and realistic DFT calculations, which, in addition to detailed comparison that can be done for the QPI from the Fermi arcs, is a hallmark of scattering between Fermi arcs. Finally, we have demonstrated that the trademark of a Fermi arc can be distinguished even in cases where the QPI pattern is a superposition of bulk and surface contributions, provided that the Fermi arc has a

prominent surface DOS. Our results suggest that there can be an unequivocal observation of Fermi-arc signatures in STS experiments.

ACKNOWLEDGMENTS

This work was supported by NSF CAREER DMR-0952428, ONR-N00014-11-1-0635, MURI-130-6082, the Packard Foundation, and the Keck grant. SK acknowledges financial support by the ICAM branch contributions. JL acknowledges support from Swiss National Science Foundation. SK is grateful to A. G. Grushin for enlightening discussions.

[1] G. E. Volovik, *The Universe in a Helium Droplet* (Clarendon, Oxford, 2003).
[2] H. B. Nielsen and M. Ninomiya, Nucl. Phys. B **185**, 20 (1981).
[3] H. B. Nielsen and M. Ninomiya, Nucl. Phys. B **193**, 173 (1981).
[4] H. B. Nielsen and M. Ninomiya, Phys. Lett. B **130**, 389 (1983).
[5] Z. Fang, N. Nagaosa, K. S. Takahashi, A. Asamitsu, R. Mathieu, T. Ogasawara, H. Yamada, M. Kawasaki, Y. Tokura, and K. Terakura, Science **302**, 92 (2003).
[6] X. Wan, A. M. Turner, A. Vishwanath, and S. Y. Savrasov, Phys. Rev. B **83**, 205101 (2011).
[7] G. Xu, H. Weng, Z. Wang, X. Dai, and Z. Fang, Phys. Rev. Lett. **107**, 186806 (2011).
[8] L. Balents, Physics (College. Park. Md). **4**, 36 (2011).
[9] B. A. Bernevig, Nat. Phys. **11**, 698 (2015).
[10] A. M. Turner and A. Vishwanath, Contemp. Concepts Condens. Matter Sci. **6**, 293 (2013).
[11] Z. Wang, Y. Sun, X. Q. Chen, C. Franchini, G. Xu, H. Weng, X. Dai, and Z. Fang, Phys. Rev. B **85**, 195320 (2012).
[12] Z. Wang, H. Weng, Q. Wu, X. Dai, and Z. Fang, Phys. Rev. B **88**, 125427 (2013).
[13] H. Weng, X. Dai, and Z. Fang, MRS Bull. **39**, 849 (2014).
[14] B. Q. Lv, H. M. Weng, B. B. Fu, X. P. Wang, H. Miao, J. Ma, P. Richard, X. C. Huang, L. X. Zhao, G. F. Chen, Z. Fang, X. Dai, T. Qian, and H. Ding, Phys. Rev. X **5**, 031013 (2015).
[15] B. Q. Lv, N. Xu, H. M. Weng, J. Z. Ma, P. Richard, X. C. Huang, L. X. Zhao, G. F. Chen, C. E. Matt, F. Bisti, V. N. Strocov, J. Mesot, Z. Fang, X. Dai, T. Qian, M. Shi, and H. Ding, Nat. Phys. **11**, 724 (2015).
[16] S.-Y. Xu, I. Belopolski, N. Alidoust, M. Neupane, G. Bian, C. Zhang, R. Sankar, G. Chang, Z. Yuan, C.-C. Lee, S.-M. Huang, H. Zheng, J. Ma, D. S. Sanchez, B. Wang, A. Bansil, F. Chou, P. P. Shibayev, H. Lin, S. Jia, and M. Z. Hasan, Science **349**, 613 (2015).
[17] S.-Y. Xu, N. Alidoust, I. Belopolski, Z. Yuan, G. Bian, T.-R. Chang, H. Zheng, V. N. Strocov, D. S. Sanchez, G. Chang, C. Zhang, D. Mou, Y. Wu, L. Huang, C.-C. Lee, S.-M. Huang, B. Wang, A. Bansil, H.-T. Jeng, T. Neupert, A. Kaminski, H. Lin, S. Jia, and M. Zahid Hasan, Nat. Phys. **11**, 748 (2015).
[18] L. X. Yang, Z. K. Liu, Y. Sun, H. Peng, H. F. Yang, T. Zhang, B. Zhou, Y. Zhang, Y. F. Guo, M. Rahn, D. Prabhakaran, Z. Hussain, S.-K. Mo, C. Felser, B. Yan, and Y. L. Chen, Nat. Phys. **11**, 728 (2015).
[19] C. Zhang, Z. Yuan, S.-Y. Xu, Z. Lin, B. Tong, M. Z. Hasan, J. Wang, C. Zhang, and S. Jia, arXiv:1502.00251 (2015).
[20] C. Zhang, S.-Y. Xu, I. Belopolski, Z. Yuan, Z. Lin, B. Tong, N. Alidoust, C.-C. Lee, S.-M. Huang, H. Lin, M. Neupane, D. S. Sanchez, H. Zheng, G. Bian, J. Wang, C. Zhang, T. Neupert, M. Z. Hasan, and S. Jia, arXiv:1503.02630 (2015).
[21] H. Weng, C. Fang, Z. Fang, B. A. Bernevig, and X. Dai, Phys. Rev. X **5**, 011029 (2015).
[22] S.-M. Huang, S.-Y. Xu, I. Belopolski, C.-C. Lee, G. Chang, B. Wang, N. Alidoust, G. Bian, M. Neupane, A. Bansil, H. Lin, and M. Z. Hasan, Nat. Commun. **6**, 7373 (2015).
[23] A. A. Soluyanov, D. Gresch, Z. Wang, Q. S. Wu, M. Troyer, X. Dai, and B. A. Bernevig, arXiv:1507.01603v1 (2015).
[24] Y. Sun, S.-C. Wu, M. N. Ali, C. Felser, and B. Yan, Phys. Rev. B **92**, 161107 (2015).
[25] Z. Wang, D. Gresch, A. A. Soluyanov, W. Xie, X. Dai, M. Troyer, R. J. Cava, and B. A. Bernevig, arXiv:1511.07440 (2015).
[26] K. McElroy, R. W. Simmonds, J. E. Hoffman, D.-H. Lee, J. Orenstein, H. Eisaki, S. Uchida, and J. C. Davis, Nature **422**, 592 (2003).
[27] P. Aynajian, E. H. da Silva Neto, A. Gyenis, R. E. Baumbach, J. D. Thompson, Z. Fisk, E. D. Bauer, and A. Yazdani, Nature **486**, 201 (2012).
[28] P. Roushan, J. Seo, C. V. Parker, Y. S. Hor, D. Hsieh, D. Qian, A. Richardella, M. Z. Hasan, R. J. Cava, and A. Yazdani, Nature **460**, 1106 (2009).
[29] T. Zhang, P. Cheng, X. Chen, J. F. Jia, X. Ma, K. He, L. Wang, H. Zhang, X. Dai, Z. Fang, X. Xie, and Q. K. Xue, Phys. Rev. Lett. **103**, 266803 (2009).
[30] J. Seo, P. Roushan, H. Beidenkopf, Y. S. Hor, R. J. Cava, and A. Yazdani, Nature **466**, 343 (2010).
[31] Y. Okada, C. Dhital, W. Zhou, E. D. Huemiller, H. Lin, S. Basak, A. Bansil, Y. B. Huang, H. Ding, Z. Wang, S. D. Wilson, and V. Madhavan, Phys. Rev. Lett. **106**, 206805 (2011).
[32] Z. Alpichshev, J. G. Analytis, J. H. Chu, I. R. Fisher, Y. L. Chen, Z. X. Shen, A. Fang, and A. Kapitulnik, Phys. Rev. Lett. **104**, 016401 (2010).
[33] Z. Alpichshev, J. G. Analytis, J. H. Chu, I. R. Fisher, and A. Kapitulnik, Phys. Rev. B **84**, 041104 (2011).
[34] C. Fang, M. J. Gilbert, S.-Y. Xu, B. A. Bernevig, and M. Z. Hasan, Phys. Rev. B **88**, 125141 (2013).
[35] D. Zhang, H. Baek, J. Ha, T. Zhang, J. Wyrick, A. V. Davydov, Y. Kuk, and J. A. Stroscio, Phys. Rev. B **89**, 245445 (2014).
[36] P. Hosur, Phys. Rev. B **86**, 195102 (2012).
[37] J. S. Hofmann, R. Queiroz, and A. P. Schnyder, Phys. Rev. B **88**, 134505 (2013).
[38] L. Capriotti, D. J. Scalapino, and R. D. Sedgewick, Phys. Rev. B **68**, 014508 (2003).
[39] P. G. Derry, A. K. Mitchell, and D. E. Logan, Phys. Rev. B **92**, 035126 (2015).
[40] G. D. Mahan, *Many-Particle Physics*, Physics of Solids and Liquids (Springer, 2000).
[41] J. E. Hoffman, K. McElroy, D.-H. Lee, K. M. Lang, H. Eisaki, S. Uchida, and J. C. Davis, Science **297**, 1148 (2002).
[42] L. Simon, F. Vonau, and D. Aubel, J. Phys. Condens. Matter **19**, 355009 (2007).
[43] See Supplemental Material for more information on calculations.
[44] Y. Sun, S.-C. Wu, and B. Yan, Phys. Rev. B **92**, 115428 (2015).

[45] There are 4 more arcs, located inside features 3 and 4 of Fig. 4(a), that are not resolved at this energy.